JACC: CARDIOVASCULAR IMAGING VOL. 7, NO. 2, 2014

ISSN 1936-878X/$36.00
PUBLISHED BY ELSEVIER INC. http://dx.doi.org/10.1016/j.jcmg.2013.12.003

PET/CT Imaging of Integrin αvβ3 Expression in Human Carotid Atherosclerosis

Ambros J. Beer, MD,* Jaroslav Pelisek, PhD,† Peter Heider, MD,† Antti Saraste, MD,‡ Christian Reeps, MD,† Stephan Metz, MD,§ Stefan Seidl, MD,‖ Horst Kessler, PhD,¶# Hans-Jürgen Wester, PhD,** Hans Henning Eckstein, MD,† Markus Schwaiger, MD*

Munich, Neuherberg, and Garching, Germany; and Jeddah, Saudi Arabia

OBJECTIVES The goal of this study was to evaluate the feasibility of [^{18}F]Galacto-RGD positron emission tomography (PET)/computed tomography (CT) imaging of αvβ3 expression in human carotid plaques.

BACKGROUND The integrin αvβ3 is expressed by macrophages and angiogenic endothelial cells in atherosclerotic lesions and thus is a marker of plaque inflammation and, potentially, of plaque vulnerability. [^{18}F]Galacto-RGD is a PET tracer binding specifically to αvβ3. Therefore, [^{18}F]Galacto-RGD PET/CT imaging of αvβ3 expression in human carotid plaques might provide a novel noninvasive biomarker of plaque vulnerability.

METHODS [^{18}F]Galacto-RGD PET/CT imaging was performed in 10 patients with high-grade carotid artery stenosis scheduled for carotid endarterectomy. Tracer uptake was measured in the stenotic areas of the carotid arteries, as well as on the contralateral side, and was corrected for blood pool activity, measured in the distal common carotid artery (target-to-background [TB] ratio). TB ratio was correlated with immunohistochemistry of αvβ3 expression (LM609), macrophage density (CD68), and microvessel density (CD31) of the surgical specimen. In addition, ex vivo autoradiography of the surgical specimen with [^{18}F]Galacto-RGD and competition experiments with an unlabeled αvβ3-specific RGD peptide were performed.

RESULTS [^{18}F]Galacto-RGD PET/CT showed significantly higher TB ratios in stenotic areas compared with nonstenotic areas ($p = 0.01$). TB ratios correlated significantly with αvβ3 expression ($R = 0.787$, $p = 0.026$) and intensity of ex vivo autoradiography ($R = 0.733$, $p = 0.038$). Binding to atherosclerotic plaques was efficiently blocked in ex vivo competition experiments. A weak-to-moderate correlation was found with macrophage density ($R = 0.367$, $p = 0.299$) and microvessel density ($R = 0.479$, $p = 0.176$), which did not reach statistical significance.

CONCLUSIONS [^{18}F]Galacto-RGD PET/CT shows specific tracer accumulation in human atherosclerotic carotid plaques, which correlates with αvβ3 expression. Based on these initial data, larger prospective studies are now warranted to evaluate the potential of molecular imaging of αvβ3 expression for assessment of plaque inflammation in patients. (J Am Coll Cardiol Img 2014;7:178–87) © 2014 by the American College of Cardiology Foundation

From the *Department of Nuclear Medicine, Technische Universität München, Munich, Germany; †Department of Vascular Surgery, Technische Universität München, Munich, Germany; ‡Turku PET Centre and Department of Cardiology, Turku, Finland; §Department of Radiology, Technische Universität München, Munich, Germany; ‖Department of Pathology, Helmholtz Zentrum München, Neuherberg, Germany; ¶Institute for Advanced Study and Center of Integrated Protein Science, Technische Universität München, Department Chemie, Garching, Germany; #Chemistry Department, Faculty of Science, King Abdulaziz University, Jeddah, Saudi Arabia; and the **Chair of Pharmaceutical Radiochemistry, Technische Universität München, Garching, Germany. This work was supported by EC-FP6-project DiMI (LSHBCT-2005-512146) and by an unrestricted grant from Bristol-Myers Squibb to Dr. Schwaiger. Dr. Schwaiger has received a Siemens PET/MR research grant. All other authors have reported that they have no relationships relevant to the contents of this paper to disclose.

Manuscript received December 4, 2013; accepted December 5, 2013.

Stroke is a leading cause of long-term disability and the fourth leading cause of death in the United States (1). Atherosclerosis is the major reason for most clinical cardiovascular events such as stroke, and inflammation is an important feature of atherosclerotic plaque progression and vulnerability (2,3). More recently, intraplaque angiogenesis has also been implicated in rapid plaque growth and plaque rupture, which are of special relevance in carotid atherosclerotic lesions (4,5). Noninvasive imaging of inflammation and angiogenesis within atherosclerotic lesions may therefore be useful to predict future risk of plaque rupture and allow monitoring of antiatherosclerotic therapies, such as with magnetic resonance imaging (MRI) (6,7). However, despite the vast improvements in plaque imaging with MRI, radiotracer approaches might still provide useful additional information because they are more focused on quantifying specific biological processes. Moreover, MRI signals are much harder to quantify compared with radiotracer techniques such as positron emission tomography (PET). Thus, PET and MRI can provide synergistic information with respect to plaque imaging, and combining the data from each technique might even further improve our knowledge of plaque biology and vulnerability (8). This information may be of special relevance for use in the now clinically available hybrid PET/MRI scanners (9).

Multiple experimental and human studies have provided evidence that PET with the use of fluorine-18-fluorodeoxyglucose ([^{18}F]FDG), a glucose analogue that is taken up by macrophages, could provide an index of inflammation in atherosclerotic lesions (10–12). In atherosclerotic lesions, both macrophages and activated endothelial cells can express high levels of the αvβ3 integrin, a cell surface glycoprotein receptor (13–16). Therefore, αvβ3 expression potentially is a combined marker of both inflammation and angiogenesis in atherosclerotic lesions. Imaging of αvβ3 integrin expression might thus be useful as a noninvasive in vivo surrogate parameter of plaque vulnerability (17,18). [^{18}F] Galacto-RGD is a peptide tracer for PET imaging with highly specific binding to the αvβ3 integrin (19). Recently, specific uptake of the αvβ3-targeted tracers [^{68}Ga]DOTA-RGD and [^{18}F]Galacto-RGD has been shown in atherosclerotic plaques in the aorta of hypercholesterolemic mice (20,21). Moreover, [^{18}F]Galacto-RGD uptake in these plaques could be reduced by diet intervention, demonstrating the potential of αvβ3 imaging for evaluation of therapy response (22). Clinically, [^{18}F] Galacto-RGD PET has been successfully validated for imaging the level of αvβ3 expression in tumors (23–25). However, most tumor lesions in patients were substantially larger than atherosclerotic lesions, and the spatial resolution of clinical PET and PET/computed tomography (CT) imaging is limited (26). Thus, the potential of imaging αvβ3 expression in atherosclerotic lesions with [^{18}F]Galacto-RGD PET in the clinical setting remains unknown.

In the present study, we evaluated the general technical feasibility of PET/CT imaging of αvβ3 expression in patients with carotid stenosis who were scheduled for endarterectomy. We correlated the in vivo uptake of [^{18}F]Galacto-RGD in carotid plaques with histopathological data and in vitro autoradiography of the surgery specimen.

METHODS

Patients. Informed written consent was obtained from all patients. The ethics committee of our university approved the study protocol. Ten patients with high-grade carotid artery stenosis scheduled for carotid endarterectomy were examined within 2 weeks before the operation with [^{18}F]Galacto-RGD PET/CT (mean age 68.5 ± 6.6 years; range 55 to 79 years). Inclusion criteria were carotid artery stenosis >70% in asymptomatic patients and carotid artery stenosis >50% in symptomatic patients. Further inclusion criteria were age >40 years and the ability to provide written and informed consent. Exclusion criteria were pregnancy, lactation period, and impaired renal function (serum creatinine level >1.2 mg/dl). All patients underwent MR angiography or CT angiography and clinical examination, including Doppler ultrasound of the carotid arteries, before operation.

ABBREVIATIONS AND ACRONYMS

CCA = common carotid artery
[^{18}F]FDG = fluorine-18-fluorodeoxyglucose
ICA = internal carotid artery
MRI = magnetic resonance imaging
ROI = region of interest
SUV = standardized uptake value
TB = target-to-background

Radiopharmaceuticals. Synthesis of the precursor and subsequent [^{18}F]-labeling of Galacto-RGD was conducted as described previously (27).

[^{18}F]Galacto-RGD PET/CT imaging. Imaging was performed with a Biograph Sensation 16 PET/CT (Siemens Medical Solution, Forchheim, Germany). Ninety minutes after injection of [^{18}F]Galacto-RGD (188 ± 19 MBq), an emission scan was performed in 3-dimensional mode in the craniocaudal direction from the floor of the mouth to the upper mediastinum (3-dimensional mode; 1 bed position, 15-min acquisition time) (Online Appendix).

Image analysis. The corrected emissions scans were calibrated to standardized uptake values (SUV)

(measured activity concentration [Bq/ml] × body weight [g]/injected activity [Bq]). Images were analyzed on a Leonardo workstation (Siemens, Erlangen, Germany). In the fused PET/CT images, a region of interest (ROI) was placed in the axial slice with the maximum tracer accumulation in projection on the site of the carotid stenosis (carotid bifurcation or internal carotid artery [ICA]) as determined using visual analysis. For determination of the location of the stenosis, PET/CT data were correlated with MR or CT angiography data. Another ROI was placed in the carotid artery on the contralateral side. Finally, another ROI was placed below the level of the carotid bifurcation in the nondiseased common carotid artery (CCA) on both sides to measure unspecific tracer retention in the blood pool. The size of the ROIs was adapted to the size of the vessels and kept smaller than the vessel diameter to minimize partial volume effects. The mean SUV of the ROIs was used for further analysis (SUV_{mean}). Target-to-background ratios (TB ratio) were calculated by using the following formula:

$$SUV_{mean}\,(\text{target})/(0.5 \times [SUV_{mean}\ \text{left CCA} + SUV_{mean}\ \text{right CCA}])$$

Results were expressed as percentage of uptake over blood pool (TB ratio in %).

Thromboendarterectomy and tissue sampling. The carotid plaque was removed by standard carotid thromboendarterectomy, excising the intimal part of the artery together with all plaque components. Tissue samples were immediately separated into segments of 3 to 4 mm, embedded in optimum cutting temperature compound (Tissue-Tek; Sakura, Zoeterwoude, the Netherlands), snap-frozen in liquid nitrogen, and stored at −70°C until further analysis.

Autoradiography. In vitro binding of ^{18}F-galacto-RGD to the carotid plaques was studied by digital autoradiography of carotid thromboendarterectomy specimen tissue sections incubated with ^{18}F-galacto-RGD in the presence or absence of an excessive amount of competing tracer, as described earlier (28) (Online Appendix).

Histological analyses. Tissues samples embedded in optimum cutting temperature compound were sectioned by using a cryostat (Leica Microsystems, Wetzlar, Germany) and placed on electrically charged glass slides. Histological features of carotid plaques were studied in tissue sections stained with hematoxylin/eosin and elastin van Gieson to assess plaque structure and morphology, elastin, and collagen content. Stained samples were analyzed by using light microscopy. Macrophages, endothelial cells, smooth muscle cells, and integrin αvβ3 were detected by immunostaining with the use of the following primary antibodies: anti-CD31 (clone JC70A, dilution 1:40; Dako, Hamburg, Germany), anti-CD68 (clone KP1, dilution 1:2,000; Dako), anti–smooth muscle actin (clone HHF35; dilution 1:200; Dako), and biotinylated goat anti-mouse anti-αvβ3 (Chemicon, Schwalbach, Germany).

After primary antibody incubation, visualization was performed using either an APAAP ChemMate or peroxidase/diaminobenzidine ChemMate Detection Kit (Dako). Biotinylated antibody against αvβ3 was detected by a streptavidin-horseradish peroxidase-complex (Jackson Immunoresearch Laboratories, West Grove, Pennsylvania) and visualized with diaminobenzidine (Sigma-Aldrich, Munich, Germany). Unspecific primary immunoglobulin G antibodies were used as negative controls. Two experienced investigators blinded to the source of each specimen analyzed all images.

Statistical analysis. Signal intensities determined for the different regions are expressed as mean ± SEM or in box-and-whisker plots. Differences between the different subgroups were evaluated by using a Mann-Whitney *U* test. For linear regression analysis, Spearman rank correlation coefficient r and the p value derived from a 2-tailed Student *t* distribution were computed. Univariate correlations were calculated using the Pearson correlation method. Statistical significance was assigned for $p < 0.05$. Computations were performed using MedCalc (MedCalc Software, Mariakerke, Belgium).

RESULTS

[^{18}F]Galacto-RGD PET/CT of atherosclerotic plaques. There were 4 sites of the carotid bifurcation or ICA without stenosis (grade 0), 4 with low-grade stenosis (grade 1), 2 with moderate stenosis (grade 2), 9 with severe stenosis (grade 3), and 1 near total occlusion (grade 4) as classified by using ultrasound and MR angiography.

In vivo PET/CT imaging demonstrated focal [^{18}F]Galacto-RGD uptake (>120% TB ratio) in 5 patients that co-localized with atherosclerotic lesions as seen on CT imaging (Fig. 1). Mean uptake of [^{18}F]Galacto-RGD was significantly higher in areas of the CCA or ICA with medium- or high-grade stenosis compared with areas with none/low-grade stenosis ($p = 0.04$). Consistent with this finding, mean uptake of [^{18}F]Galacto-RGD was significantly higher in areas of the CCA or ICA with a flow velocity >150 cm/s as determined by Doppler ultrasound (Fig. 2).

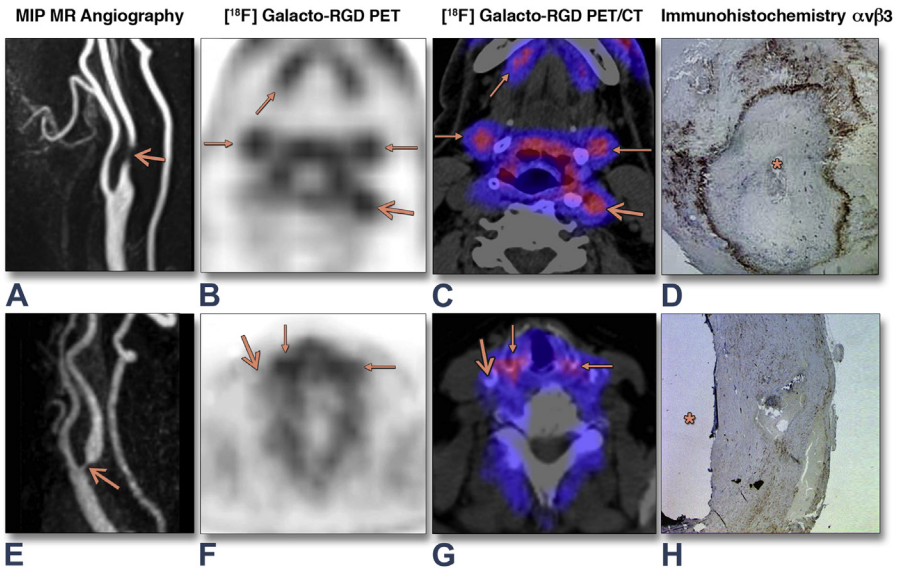

Figure 1. Patterns of [^{18}F]Galacto-RGD Uptake in High-Grade Stenosis

Comparison of 2 patients with high-grade stenosis of the internal carotid artery (ICA) on the left side (**A** to **D**, patient A) and right side (**E** to **H**, patient B). In magnetic resonance (MR) angiography, one can assess the extent of stenosis (**A** and **E**; **arrows, open tip**). The patient with the left ICA stenosis exhibits focal uptake in the plaque (**B**, positron emission tomography (PET) alone; **C**, PET/computed tomography (CT); **arrows, open tip**), whereas the patient with stenosis on the right side does not exhibit elevated uptake in the site of stenosis (**F**, PET alone; **G**, PET/CT; **arrows, open tip**). Note the physiological radiotracer uptake in the salivary glands (submandibular and sublingual glands in **B** and **C**; **arrows, closed tip**) and in the mucosal lining of the pharynx and larynx (**B**, **C**, **F**, and **G**; **arrows, closed tip**). Immunohistochemistry of αvβ3 expression in the advanced carotid atherosclerotic plaques (**G** and **H**) demonstrate strongly elevated αvβ3 expression in the plaque in patient A, whereas there is only little αvβ3 expression in the plaque in patient B (lumen is marked by **asterisk**). Bar = 100 μm.

However, in the group with medium- or high-grade stenosis (or higher flow velocity), there was a wide distribution of tracer uptake, also with no or little uptake in some stenotic areas.

Correlation to histology. As shown in Figure 3, histological correlates of [^{18}F]Galacto-RGD uptake were studied in serial tissue sections of the thromboendarterectomy specimen. CD31 as a pan-endothelial marker demonstrated a strong positive signal in the endothelial lining of the plaques and on the plaque neovasculature. CD68 as a marker for macrophages demonstrated macrophage infiltration

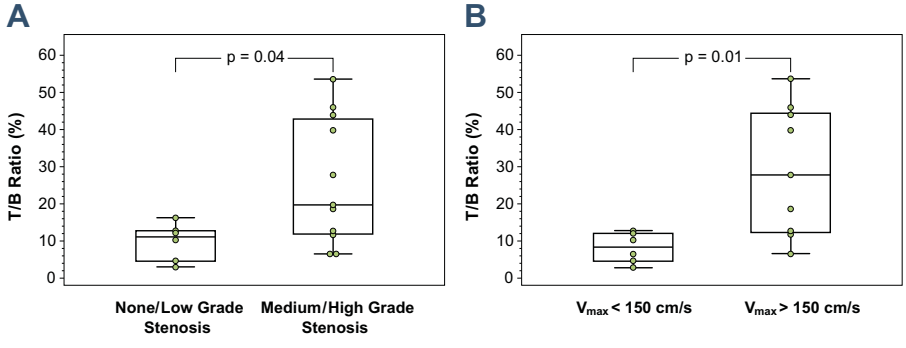

Figure 2. Analysis of [^{18}F]Galacto-RGD Uptake

Box-and-whisker plots of the tracer uptake of [^{18}F]Galacto-RGD in PET/CT measured as target-to-background ratio in the areas of no/low-grade stenosis or medium- and high-grade stenosis **(A)**. In **B**, the corresponding values are stratified according to flow velocity as measured by Doppler ultrasound in the area of stenosis (cutoff 150 cm/s). Note that tracer uptake was significantly higher in areas of medium- and high-grade stenosis and correspondingly in areas with elevated blood flow. V_{max} = maximum initial velocity; other abbreviations as in Figure 1.

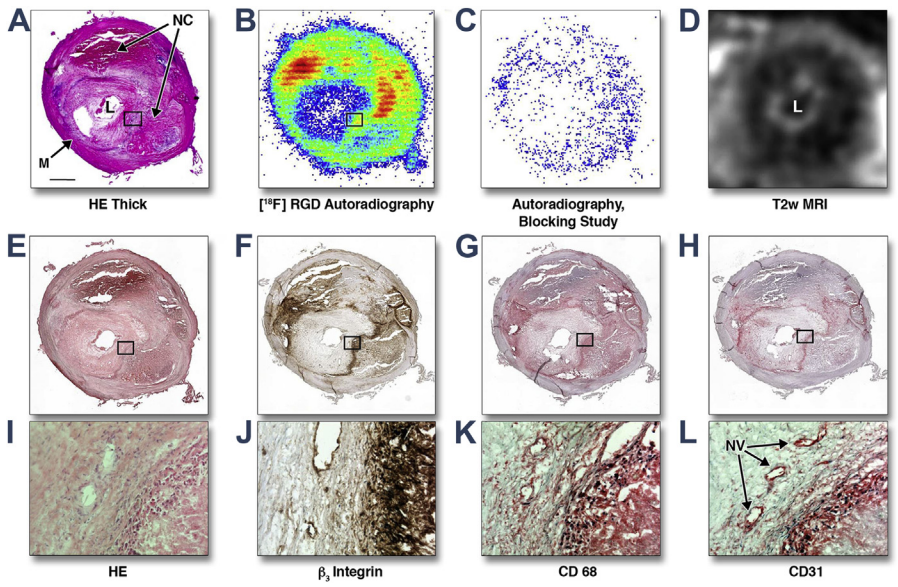

Figure 3. Autoradiography and Immunohistochemistry

Autoradiography and immunohistochemistry studies of the plaque of patient A in Figure 1 (**A**, thick section; **E**, thin section; **I**, magnification). **D** shows the T2-weighted axial magnetic resonance imaging (MRI) for comparison, which also shows different layers of plaque composition. In vitro binding and competition experiments demonstrated specific binding of [^{18}F]Galacto-RGD to αvβ3 integrin in the plaques on tissue sections **(B)**. The binding was efficiently blocked on a serial tissue section in the presence of unlabeled cyclic RGD **(C)**. Areas showing the highest RGD binding **(yellow and red)** exhibited a high degree of β3 integrin expression (**F** and **J**), macrophage infiltration (**G** and **K**), and neovascularization (**H** and **L**; **arrows**). Scale bar 1 mm in **A** to **H** and 75 μm in **I** to **L**. L = lumen; M = rest of media remained after carotid plaque excision; NC = large necrotic core with lipid deposition and hemorrhage; NV = neovessels; other abbreviations as in Figure 1.

in the plaques to a variable extent. Immunohistochemical staining for αvβ3 demonstrated αvβ3 expression on endothelial cells of intraplaque neovasculature, as well as macrophages. [^{18}F]Galacto-RGD uptake (TB ratio) correlated significantly with αvβ3 expression ($R = 0.787$, $p = 0.026$). There was a weak-to-moderate correlation with macrophage infiltration ($R = 0.367$, $p = 0.299$), intraplaque neovasculature ($R = 0.479$, $p = 0.176$), and total plaque cellularity ($R = 0.488$, $p = 0.168$) that did not reach statistical significance (Fig. 4). There was no significant correlation with intraplaque elastin ($R = 0.311$, $p = 0.380$) or collagen content ($R = 0.026$, $p = 0.941$). Due to the limited quality of our fresh frozen specimens, no systematic analysis of plaque composition was feasible.

Binding of [^{18}F]Galacto-RGD to atherosclerotic plaques in vitro. Binding of [^{18}F]Galacto-RGD in atherosclerotic plaques was studied by using ex vivo autoradiography of the thromboendarterectomy specimen and compared with in vivo tracer uptake and immunohistochemistry. Specificity of [^{18}F]Galacto-RGD binding in the atherosclerotic plaques was verified in a displacement study (Figs. 3B and 3C). [^{18}F]Galacto-RGD was found to bind to the atherosclerotic lesions to a variable extent (mean PSL/mm^2 = 80.0 ± 26.2), and the binding was efficiently and significantly reduced in the presence of an inhibitor, an unlabeled cyclic αvβ3-specific RGD peptide (mean PSL/mm^2 = 10.4 ± 3.1). The ratio of specific to nonspecific binding was approximately 8-fold (7.9 ± 2.0). In vitro [^{18}F]Galacto-RGD binding to the plaques correlated strongly and significantly with the score of αvβ3 expression in the corresponding slices of the specimen ($R = 0.913$, $p = 0.010$). Moreover, in vitro [^{18}F]Galacto-RGD binding to the plaques also correlated significantly with in vivo [^{18}F]Galacto-RGD uptake as measured by using PET/CT imaging ($R = 0.733$, $p = 0.038$). These data suggest that in vivo uptake of [^{18}F]Galacto-RGD in PET/CT is specific and correlated with αvβ3 expression in atherosclerotic lesions.

Uptake of [^{18}F]Galacto-RGD in symptomatic and asymptomatic lesions. According to the presence of patient symptoms probably caused by carotid stenosis, lesions were classified as either symptomatic ($n = 5$) or asymptomatic ($n = 11$). There was no

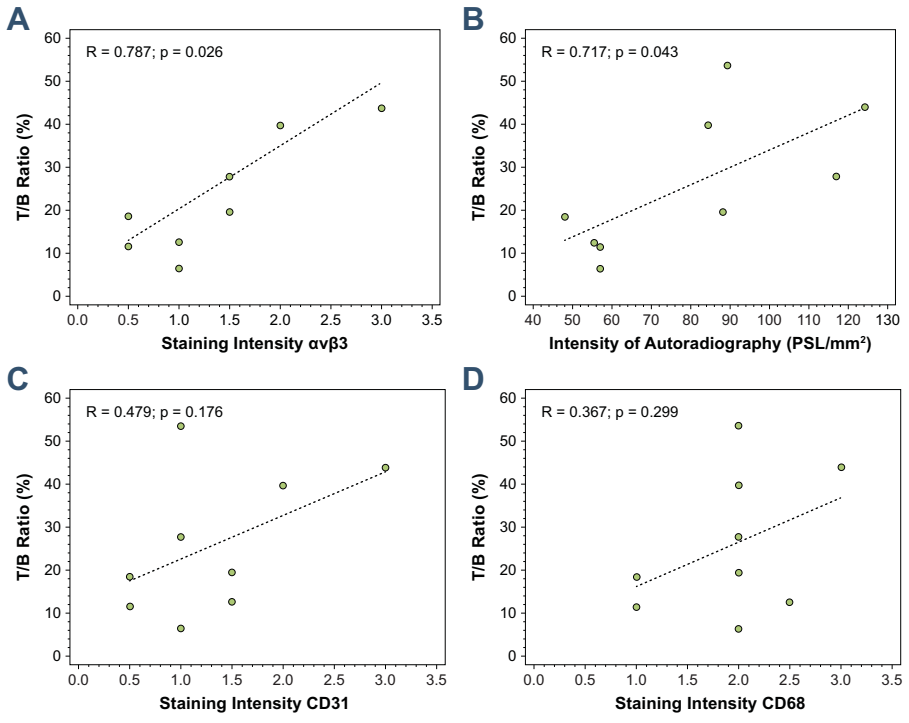

Figure 4. Correlation of Tracer Uptake and Immunohistochemistry

Linear regression analysis of [^{18}F]Galacto-RGD uptake in PET/CT measured as target-to-background (TB) ratio and **(A)** staining intensity of αvβ3 expression, **(C)** endothelial cells (CD31), and **(D)** macrophages (CD68). **(B)** Shows the correlation of in vivo tracer uptake with the intensity of autoradiography in vitro. Note that there is a significant correlation of in vivo tracer uptake and αvβ3 expression, as well as tracer uptake in vivo and in vitro autoradiography. Abbreviations as in Figure 1.

significant difference in [^{18}F]Galacto-RGD uptake in PET/CT imaging in symptomatic (mean TB ratio 21.3 ± 16.7%) or asymptomatic (mean TB ratio 17.8 ± 15.5%; p = 0.70) lesions (Fig. 5).

DISCUSSION

In this study, we demonstrate for the first time the feasibility of [^{18}F]Galacto-RGD PET/CT imaging to show focal increases in αvβ3 integrin expression in atherosclerotic plaques in patients with high-grade carotid stenosis. [^{18}F]Galacto-RGD uptake significantly correlated with intraplaque αvβ3 expression and autoradiography and could be specifically blocked in in vitro competition experiments. On the basis of these initial data, future studies on PET/CT imaging of αvβ3 integrin expression are now warranted to further evaluate its role in patients as a potential biomarker for inflammatory activity of atherosclerotic lesions.

[^{18}F]Galacto-RGD uptake in atherosclerotic plaques. [^{18}F]Galacto-RGD is a tracer that is based on the cyclic pentapeptide cyclo(-ARG-Gly-Asp-D-Phe-Val-) developed by Heckmann and Kessler (29). It shows high affinity and selectivity for αvβ3 integrin in vitro as well as receptor-type specific accumulation in vivo in αvβ3 integrin–positive tumors in mouse models and humans (18,23,27). Studies have indicated sufficient signal intensity for visualizing increased αvβ3 integrin expression in benign lesions such as infarcted myocardium (30,31). However, up to now, it was unknown whether αvβ3 expression in human carotid plaques is sufficient for imaging with [^{18}F]Galacto-RGD PET. In this study, we found that focal [^{18}F]Galacto-RGD uptake can be visualized in atherosclerotic lesions in patients by using PET/CT imaging. As expected, the mean uptake of [^{18}F]Galacto-RGD in atherosclerotic lesions was several folds lower than reported for αvβ3 integrin–expressing tumors (32–34). This can easily be explained by the small volume even of relatively large atherosclerotic plaques compared with most tumor lesions, which usually were >20 mm in diameter in the reported studies. Because the spatial

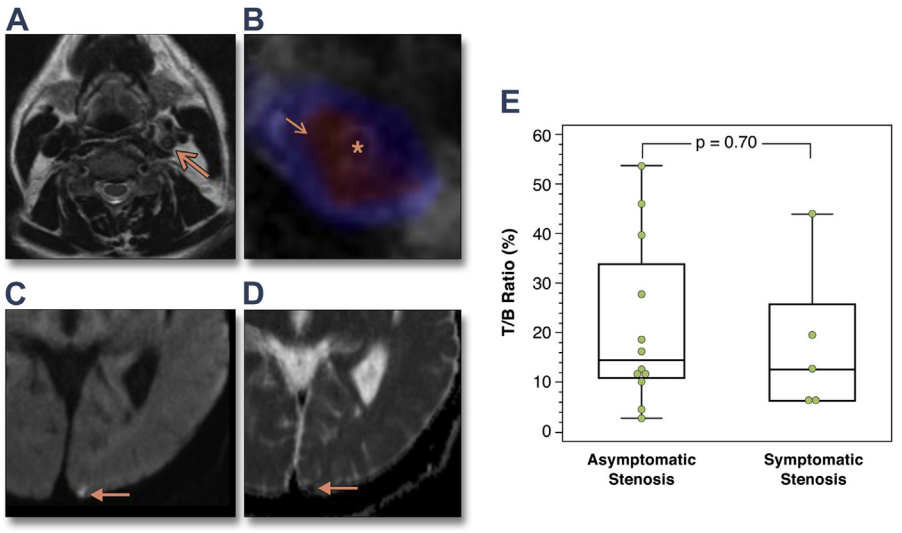

Figure 5. Correlation of Tracer Uptake and Patient Symptoms

Acute ipsilateral cortical ischemia in a patient with intense [^{18}F]Galacto-RGD uptake in a vulnerable carotid plaque. **(A)** shows the plaque of the patient with the high-grade stenosis of the left ICA in Figure 1 in a T2-weighted axial MRI slice **(arrow, open tip)**. The MRI-PET image fusion **(B)**, which is zoomed in on the stenotic left ICA seen in **A**, shows the tracer uptake in the plaque, which corresponds to the pattern of tracer uptake in autoradiography in Figure 3B (**arrow, open tip**; lumen, **asterisk**). This patient had an acute small ischemia as demonstrated by diffusion-weighted MRI (in the ipsilateral left parietal cortex [**arrow**; **C**, b1000 image; **D**, apparent diffusion coefficient map]), proving that the plaque was vulnerable. However, when analyzing all patients for symptomatic or asymptomatic stenosis, there was no significant difference notable between groups **(E)**. Abbreviations as in Figures 1 and 3.

resolution of PET is limited, the so-called partial volume effect artificially reduces the measured uptake in lesions smaller than approximately 20 to 25 mm (35). However, despite the small size of atherosclerotic lesions, our results suggest that visualization of αvβ3 integrin expression in human plaques is generally possible with PET/CT imaging by using αvβ3-specific tracers. It has to be noted, however, that in our small patient population, the correlation was relatively loose, so up to now it has not been clear to what extent tracer uptake and αvβ3 expression correlate linearly. This is also somewhat related to the relatively low signal achieved. To improve uptake and TB ratios, tracer optimization by multimerization has been shown to increase signal intensity from αvβ3 integrin–expressing tissues (36). Moreover, sophisticated algorithms for partial volume correction might improve the results from PET and PET/CT imaging (37).

Immunohistochemical correlate of [^{18}F]Galacto-RGD uptake. Histological and immunohistochemical analysis demonstrated that uptake of [^{18}F]Galacto-RGD significantly correlated with αvβ3 expression in the plaques, which was mainly expressed on macrophages as well as neovasculature. [^{18}F]Galacto-RGD uptake did not show a correlation with intraplaque elastin, collagen, or cellularity. A weak-to-moderate correlation was found with macrophage density and neovascularization, which did not reach statistical significance. The low number of samples in the study might, in part, have caused this, as various preclinical studies have shown a correlation of αvβ3 integrin–targeted RGD peptides with intraplaque macrophage density and/or neovascularization (20,38). However, mice models often show no substantial intraplaque neovascularization, limiting direct comparability with human atherosclerotic lesions (39–41). In preclinical MRI studies, enhancement of atherosclerotic vessel wall by αvβ3 integrin–targeted nanoparticles was mainly explained by the presence of angiogenic vessels around the intima (42). However, MRI nanoparticles remain mainly intravascular due to their larger size compared with small peptide PET tracers; thus, they do not target intraplaque macrophages, limiting direct comparability to our results.

In vitro autoradiography. In vitro autoradiography of the thromboendarterectomy specimen with [^{18}F]Galacto-RGD was performed because the specificity of tracer uptake can be demonstrated with blocking studies by pre-incubating with excess of unlabeled target specific ligands. Moreover, the

pattern of tracer distribution can be compared with immunohistochemistry.

Indeed, [^{18}F]Galacto-RGD uptake could efficiently and significantly be blocked by an unlabeled αvβ3-specific cyclic RGD peptide in vitro. Moreover, in vivo uptake of [^{18}F]Galacto-RGD measured by using PET/CT correlated significantly with in vitro autoradiography, which again correlated strongly and significantly with αvβ3 expression in the respective slices used for autoradiography. The more moderate correlation of in vivo [^{18}F]Galacto-RGD uptake and αvβ3 expression compared with in vitro autoradiography and αvβ3 expression might be explained by factors additionally influencing measured tracer uptake in PET/CT imaging in patients (e.g., lesion size, partial volume effects, tracer access to the intraplaque structures) (43).

The data strongly suggest that in vivo uptake of [^{18}F]Galacto-RGD measured by using PET/CT is specific and allows for at least semi-quantitative noninvasive assessment of the level of αvβ3 expression in atherosclerotic lesions.

Comparison to other imaging modalities. PET with [^{18}F]FDG is currently the best-characterized radiotracer approach for imaging plaque inflammation (44). Compared with [^{18}F]FDG PET, TB ratios in our study were in the range or only slightly lower compared with reported data (11,12). Moreover, a recent preclinical study compared [^{18}F]Galacto-RGD uptake with ^{3}H-DG, an in vitro analogue of [^{18}F]FDG, and uptake ratios between plaque and normal vessel wall were comparable for both tracers (20). Compared with [^{18}F]FDG, which is only taken up by intraplaque macrophages, [^{18}F]Galacto-RGD targets both macrophages and intraplaque neovasculature, which have both been implicated in progression and rupture of atherosclerotic lesions. Moreover, αvβ3 integrin may be directly involved in the degradation of the protective fibrous cap of atherosclerotic lesions because it has been identified as a binding moiety that localizes protease activity, particularly matrix metalloproteinase 2, to the cell surface (45,46). Therefore, [^{18}F]Galacto-RGD PET/CT visualizes several important features of plaque instability simultaneously, which might potentially be advantageous compared with [^{18}F]FDG (47).

In terms of imaging of αvβ3 expression with MRI, the higher resolution of MRI combined with excellent soft tissue contrast is an advantage compared with PET (42,48). However, in MRI, larger absolute amounts of probes usually have to be used compared with PET. Thus, adverse effects of most PET tracers are limited or not present at all. This facilitates translation of results of PET tracers into the clinical setting, as was successfully demonstrated for [^{18}F]Galacto-RGD in this study.

Study limitations. Because it was uncertain whether a reliable PET signal could be achieved in patients with atherosclerotic lesions, the present study was deliberately intended as a feasibility study with a limited number of patients. However, even in this small sample, a significant correlation of [^{18}F]Galacto-RGD uptake and αvβ3 expression as well as autoradiography could be demonstrated. It is beyond the scope of this study to clarify in detail the ultimate clinical value of PET/CT imaging of αvβ3 expression for identifying patients with vulnerable plaques. The value of such imaging must be addressed by future larger, prospective studies.

Moreover, due to the unavailability of αvβ3 antibody for formalin-fixed and paraffin-embedded samples, we were forced to use fresh frozen tissue for immunohistochemical analyses, which generally (especially regarding atherosclerotic tissue) result in markedly lower histological quality. Thus, assessment of plaque stability according to histopathology was not possible due to the limited quality of the specimen, which is an important topic to be clarified in future studies. However, macrophage content and neovascularization could be assessed, which are also considered to be crucial factors for plaque vulnerability.

CONCLUSIONS

We demonstrated that [^{18}F]Galacto-RGD PET/CT specifically visualizes elevated integrin αvβ3 expression in human carotid plaques. On the basis of these promising preliminary results, further prospective studies must now be conducted to define the clinical value of PET/CT or even PET/MR imaging of αvβ3 expression for assessment of plaque vulnerability and patient prognosis concerning development of symptomatic stenosis.

Acknowledgments

The authors thank the entire PET/CT and cyclotron team for assistance and Renate Hegenloh for histological staining.

Reprint requests and correspondence: Dr. Ambros J. Beer, Department of Nuclear Medicine, Klinikum rechts der Isar, Technische Universität München, Ismaninger Strasse 22, 81675 Munich, Germany. *E-mail: ambros.beer@tum.de.*

REFERENCES

1. Go AS, Mozaffarian D, Roger VL, et al. Heart disease and stroke statistics—2013 update: a report from the American Heart Association. Circulation 2013;127:e6–245.
2. Ross R. Atherosclerosis: an inflammatory disease. N Engl J Med 1999; 340:115–26.
3. Libby P. Inflammation in atherosclerosis. Nature 2002;420:868–74.
4. Virmani R, Kolodgie FD, Burke AP, et al. Atherosclerotic plaque progression and vulnerability to rupture: angiogenesis as a source of intraplaque hemorrhage. Arterioscler Thromb Vasc Biol 2005;25:2054–61.
5. Vicenzini E, Giannoni MF, Benedetti-Valentini F, Lenzi GL. Imaging of carotid plaque angiogenesis. Cerebrovasc Dis 2009;27 Suppl 2:48–54.
6. Hatsukami TS, Yuan C. MRI in the early identification and classification of high-risk atherosclerotic carotid plaques. Imaging Med 2010;2:63–75.
7. Sun J, Underhill HR, Hippe DS, Xue Y, Yuan C, Hatsukami TS. Sustained acceleration in carotid atherosclerotic plaque progression with intraplaque hemorrhage: a long-term time course study. J Am Coll Cardiol Img 2012;5:798–804.
8. Truijman MT, Kwee RM, van Hoof RH, et al. Combined 18F-FDG PET-CT and DCE-MRI to assess inflammation and microvascularization in atherosclerotic plaques. Stroke 2013;44:3568–70.
9. Ripa RS, Knudsen A, Hag AM, et al. Feasibility of simultaneous PET/MR of the carotid artery: first clinical experience and comparison to PET/CT. Am J Nucl Med Mol Imaging 2013;3:361–71.
10. Tawakol A, Migrino RQ, Bashian GG, et al. In vivo 18F-fluorodeoxyglucose positron emission tomography imaging provides a noninvasive measure of carotid plaque inflammation in patients. J Am Coll Cardiol 2006;48:1818–24.
11. Rudd JHF, Fayad ZA. Imaging atherosclerotic plaque inflammation. Nat Clin Pract Cardiovasc Med 2008; Suppl 2:S11–7.
12. Rudd J, Warburton E, Fryer T, et al. Imaging atherosclerotic plaque inflammation with [18F]-fluorodeoxyglucose positron emission tomography. Circulation 2002;105:2708–11.
13. Hoshiga M, Alpers CE, Smith LL, Giachelli CM, Schwartz SM. Alpha-v-beta-3 integrin expression in normal and atherosclerotic artery. Circ Res 1995;77:1129–35.
14. Antonov AS, Kolodgie FD, Munn DH, Gerrity RG. Regulation of macrophage foam cell formation by {alpha}V{beta}3 integrin: potential role in human atherosclerosis. Am J Pathol 2004;165:247–58.
15. Brooks PC, Clark RA, Cheresh DA. Requirement of vascular integrin alpha v beta 3 for angiogenesis. Science 1994;264:569–71.
16. Brooks PC, Montgomery AM, Rosenfield M, et al. Integrin alpha v beta 3 antagonists promote tumor regression by inducing apoptosis of angiogenic blood vessels. Cell 1994;79: 1157–64.
17. Saraste A, Nekolla SG, Schwaiger M. Cardiovascular molecular imaging: an overview. Cardiovasc Res 2009;83: 643–52.
18. Razavian M, Marfatia R, Mongue-Din H, et al. Integrin-targeted imaging of inflammation in vascular remodeling. Arterioscler Thromb Vasc Biol 2011;31:2820–6.
19. Haubner R, Wester H, Weber WA, et al. Noninvasive imaging of αvβ3 integrin expression using 18F-labeled RGD-containing glycopeptide and positron emission tomography. Cancer Res 2001;61:1781–5.
20. Laitinen I, Saraste A, Weidl E, et al. Evaluation of {alpha}v{beta}3 integrin-targeted positron emission tomography tracer 18F-Galacto-RGD for imaging of vascular inflammation in atherosclerotic mice. Circ Cardiovasc Imaging 2009;2:331–8.
21. Haukkala J, Laitinen I, Luoto P, et al. 68Ga-DOTA-RGD peptide: biodistribution and binding into atherosclerotic plaques in mice. Eur J Nucl Med Mol Imaging 2009;36:2058–67.
22. Saraste A, Laitinen I, Weidl E, et al. Diet intervention reduces uptake of αvβ3 integrin-targeted PET tracer 18F-galacto-RGD in mouse atherosclerotic plaques. J Nucl Cardiol 2012; 19:775–84.
23. Haubner R, Weber WA, Beer AJ, et al. Noninvasive visualization of the activated alphavbeta3 integrin in cancer patients by positron emission tomography and [18F]Galacto-RGD. PLoS Med 2005;2:e70.
24. Beer AJ, Haubner R, Sarbia M, et al. Positron emission tomography using [18F]Galacto-RGD identifies the level of integrin αvβ3 expression in man. Clinical Cancer Res 2006;12:3942–9.
25. Beer AJ, Grosu A, Carlsen J, et al. [18F]Galacto-RGD positron emission tomography for imaging of αvβ3 expression on the neovasculature in patients with squamous cell carcinoma of the head and neck. Clin Cancer Res 2007;13:6610–6.
26. Weber WA, Grosu AL, Czernin J. Technology insight: advances in molecular imaging and an appraisal of PET/CT scanning. Nat Clin Pract Oncol 2008;5:160–70.
27. Haubner R, Kuhnast B, Mang C, et al. [18F]Galacto-RGD: synthesis, radiolabeling, metabolic stability, and radiation dose estimates. Bioconjug Chem 2004;15:61–9.
28. Laitinen I, Marjamäki P, Någren K, et al. Uptake of inflammatory cell marker [11C]PK11195 into mouse atherosclerotic plaques. Eur J Nucl Med Mol Imaging 2009;36:73–80.
29. Heckmann D, Kessler H. Design and chemical synthesis of integrin ligands. Available at: http://www.sciencedirect.com/science/article/B7CV2-4PD42DK-P/2/c3b8f51c50831b0c617b99295c580b20. Accessed December 27, 2013.
30. Pichler BJ, Kneilling M, Haubner R, et al. Imaging of delayed-type hypersensitivity reaction by PET and 18F-Galacto-RGD. J Nucl Med 2005;46: 184–9.
31. Makowski MR, Ebersberger U, Nekolla S, Schwaiger M. In vivo molecular imaging of angiogenesis, targeting αvβ3 integrin expression, in a patient after acute myocardial infarction. Eur Heart J 2008;29:2201.
32. Beer AJ, Haubner R, Goebel M, et al. Biodistribution and pharmacokinetics of the {alpha}v{beta}3-selective tracer 18F-Galacto-RGD in cancer patients. J Nucl Med 2005;46:1333–41.
33. Beer AJ, Lorenzen S, Metz S, et al. Comparison of integrin αvβ3 expression and glucose metabolism in primary and metastatic lesions in cancer patients: a PET study using ^{18}F-Galacto-RGD and ^{18}F-FDG. J Nucl Med 2008;49:22–9.
34. Beer AJ, Niemeyer M, Carlsen J, et al. Patterns of {alpha}v{beta}3 expression in primary and metastatic human breast cancer as shown by 18F-Galacto-RGD PET. J Nucl Med 2008;49:255–9.
35. Brix G, Bellemann ME, Hauser H, Doll J. Recovery coefficients for the quantification of the arterial input functions from dynamic PET measurements: experimental and theoretical determination. Nuklearmedizin 2002;41:184–90.
36. Thumshirn G, Hersel U, Goodman SL, Kessler H. Multimeric cyclic RGD peptides as potential tools for tumor targeting: solid-phase peptide synthesis and chemoselective

oxime ligation. Chemistry 2003;9:2717–25.

37. Izquierdo-Garcia D, Davies JR, Graves MJ, et al. Comparison of methods for magnetic resonance-guided [18-F]Fluorodeoxyglucose positron emission tomography in human carotid arteries: reproducibility, partial volume correction, and correlation between methods. Stroke 2009;40:86–93.
38. Waldeck J, Hager F, Holtke C, et al. Fluorescence reflectance imaging of macrophage-rich atherosclerotic plaques using an {alpha}v{beta}3 integrin-targeted fluorochrome. J Nucl Med 2008;49:1845–51.
39. Moulton KS, Heller E, Konerding MA, Flynn E, Palinski W, Folkman J. Angiogenesis inhibitors endostatin or TNP-470 reduce intimal neovascularization and plaque growth in apolipoprotein E-deficient mice. Circulation 1999;99:1726–32.
40. Moulton KS, Vakili K, Zurakowski D, et al. Inhibition of plaque neovascularization reduces macrophage accumulation and progression of advanced atherosclerosis. PNAS 2003;100:4736–41.
41. Heinonen SE, Leppanen P, Kholova I, et al. Increased atherosclerotic lesion calcification in a novel mouse model combining insulin resistance, hyperglycemia, and hypercholesterolemia. Circ Res 2007;101:1058–67.
42. Winter PM, Morawski AM, Caruthers SD, et al. Molecular imaging of angiogenesis in early-stage atherosclerosis with {alpha}v{beta}3-integrin-targeted nanoparticles. Circulation 2003;108:2270–4.
43. Weber WA. Positron emission tomography as an imaging biomarker. J Clin Oncol 2006;24:3282–92.
44. Rudd JH, Narula J, Strauss HW, et al. Imaging atherosclerotic plaque inflammation by fluorodeoxyglucose with positron emission tomography: ready for prime time? J Am Coll Cardiol 2010;55:2527–35.
45. van Hinsbergh VW, Engelse MA, Quax PH. Pericellular proteases in angiogenesis and vasculogenesis. Arterioscler Thromb Vasc Biol 2006;26:716–28.
46. Brooks PC, Strömblad S, Sanders LC, et al. Localization of matrix metalloproteinase MMP-2 to the surface of invasive cells by interaction with integrin [alpha]v[beta]3. Cell 1996;85:683–93.
47. Weng S, Zemany L, Standley KN, et al. β3 integrin deficiency promotes atherosclerosis and pulmonary inflammation in high-fat-fed, hyperlipidemic mice. PNAS 2003;100:6730–5.
48. Burtea C, Laurent S, Murariu O, et al. Molecular imaging of αvβ3 integrin expression in atherosclerotic plaques with a mimetic of RGD peptide grafted to Gd-DTPA. Cardiovasc Res 2008;78:148–57.

Key Words: biomarker ■ carotid stenosis ■ imaging ■ molecular imaging ■ plaque.

▶ APPENDIX

For an expanded Methods section, please see the online version of this article.